Experimental Validation of End-Effector Stabilization for Underwater Vehicle-Manipulator Systems in Subsea Operations

Bent Oddvar A. Haugaløkken[1], Erlend K. Jørgensen[1], Ingrid Schjølberg[1]

Abstract— **This paper considers the kinematic control approach for controlling an underwater vehicle-manipulator system. Three different kinematic control schemes have been applied, and the performance of each scheme is compared. The kinematic control schemes provide velocity references, while the control system aims to keep a fixed position for the manipulator's end-effector, and at the same time compensate for slowly varying motions of the underwater vehicle. Experimental results show that the proposed full modified kinematic control scheme has better performance than the decoupled kinematic control scheme, while it nicely outperforms the full kinematic control scheme. All the control schemes are good alternatives for controlling an underwater vehicle-manipulator system using kinematic control.**

1. Introduction

Underwater Vehicle-Manipulator Systems (UVMS) are commonly used to perform inspection, maintenance and repair (IMR) operations on underwater structures. Increasing autonomy in these operations can potentially reduce costs and increase safety [1]. The usual approach in the offshore industry today is to have at least two operators to stabilize the UVMS body, and one operator performing the desired manipulator task. Cameras located on the vehicle and a wide array of high-accuracy sensors are often available, such as gyroscopes, accelerometers, pressure and temperature sensors, which provide the operators with information related to the state of the UVMS and the operation. Controlling the UVMS accurately requires operator skill and experience, and can be very challenging when the UVMS is subjected to disturbances. These types of operations have a potential for higher degrees of autonomy, and autonomy in IMR operations has therefore received increased interest in recent years [2][3][4].

A UVMS consists of a vehicle body, one or more manipulator arms and, typically, a cable for power and/or communication to topside. In a scenario in which the end-effector of the manipulator arm is performing some intervening task on a structure, it is crucial to keep the deviation from the desired state as small as possible. Even small deviations from setpoint may cause damage to the vehicle, the manipulator and the structure. A UVMS with n DOF manipulator arm has $6 + n$ DOFs. Consequently, a UVMS system is a kinematically redundant system, meaning the system has more DOFs than the task one wishes to control. A common approach for controlling kinematically redundant systems is kinematic control [5]. Kinematic control is a control strategy

[1]Bent Oddvar A. Haugaløkken, Erlend K. Jørgensen and Ingrid Schjølberg, Department of Marine Technology, University of Science and Technology (NTNU), 7491 Trondheim, Norway

in which the kinematic relations of the system are considered by using the Jacobians of the system and the pseudo-inverses of the Jacobians. Given a desired velocity for the end-effector, usually inversely proportional to the error for a constant setpoint, the desired velocity for each degree of freedom of the system are generated. These desired velocities are followed by a low level controller.

Controlling a manipulator arm using kinematic control has been applied successfully for a wide range of manipulator arms [6], [7]. However, for a UVMS both the vehicle body and the manipulator arm should be considered in the control scheme, and this was first carried out in the SAUVIM project [8]. The degrees of freedom for the vehicle body have very different characteristics compared to the degrees of freedom for the manipulator arm when it comes to inertia and accuracy in state estimates and actuation. The vehicle body state is commonly estimated through aided inertial navigation, it is actuated by thrusters and has a large inertia. This makes it very challenging to follow reference velocities accurately in a real scenario. Manipulator arms often have very accurate encoders to determine state and have a low inertia, yielding highly accurate control. Consequently, it is of interest to investigate whether or not the manipulator arm can compensate for the disturbances and inaccuracies that occur when controlling the UVMS body. This has been done in the MARIS [9] and TRIDENT [10] projects with great results. MARIS [9] considered a pipe grasping scenario, and compared the results of two kinematic control strategies. In the first one, only a camera video feedback was employed and a full kinematic control scheme with several tasks was implemented; in the second scheme, the arm was compensating the vehicle tracking errors thanks to the use of a DVL for estimating the actual vehicle velocity. However, in [9] the comparison has been done based on grasping success rate only. In this work we aim to numerically evaluate the reference generation techniques for the purpose of vehicle and manipulator reference velocity tracking, which was considered in [11], but only through numerical simulations.

In [12], an approach for achieving additional control objectives called *task-priority redundancy resolution* is suggested, later used in this paper. An approach in which the total hydrodynamic drag of the system is minimized is suggested in [13], and a model-based controller is chosen as the low level controller. In [14] a model-based approach is suggested, in which an indirect adaptive controller is employed, using an Extended Kalman Filter (EKF) for estimation of states and unknown parameters. The control algorithm suggested

in [15] employs a $\mathcal{H}_\infty$ optimal controller with a disturbance observer for tracking control, and use kinematic control to minimize restoring moments. A technique for performing the intervention tasks *turn a valve* and *push a button* is given in [16]. This work can be extended by introducing a way to maintain stability during manipulator operations, e.g., by implementing the zero moment point methodology described in [17]. A very recent work dedicated to motion planning for underwater vehicle-manipulator systems are presented in [18] Some earlier approaches of manipulator arm control can be seen in [19][20][21][22][23], with more recent approaches presented in [24][25][26][27][28] and a recent literature survey in [29].

It is important to note that most of the literature regarding kinematic control for underwater vehicles has been focusing on formulating different tasks to achieve various objectives and verifying the approach. This is done by either assuming reference velocities are followed perfectly or through simulations in which the kinetic model is fully known, using a model-based controller for low level control. A UVMS is a very complex and interconnected system, and mathematical modelling of the UVMS accurately in a real scenario is quite challenging, if not impossible [5]. Modelling added mass, dissipative and restoring forces is especially difficult. Furthermore, when generating reference velocities in the kinematic control scheme it is assumed that the generated reference velocities for each degree of freedom is followed perfectly. This is a valid assumption in simulation, and may also be somewhat valid in a real life scenario, depending on how the system is modelled and how it behaves.

In real case scenarios, controlling the UVMS is typically done independent of kinetic model knowledge. For low level velocity control it is possible to use a control scheme in which the model is not taken into account, such as a sliding mode controller [30][31]. However, if such a model of the vehicle is attained, model-based controllers presented in, e.g., [13] or [14], can be used. Using a sliding mode controller requires no knowledge about the kinetic model and is very robust, but naturally leads to larger deviations in tracking error, as the kinetic model information is not taken into account. Furthermore, some approaches with UVMS control through experimental validation have been suggested. The work presented in [32] performs experiments in a basin trying to stabilize the end-effector while the manipulator base is affected by translational motion. The base position is predicted based on a linear model employing velocity and specific force estimates. Inverse kinematics are used for finding desired joint angles, and a PD controller is used for joint velocity control. [33] presents a dynamic workspace control method for precise linear motion control of a manipulator's end-effector when the base is affected by disturbances. An EKF is used for state estimation and prediction, and measured sensor data is used for simulations.

The main contributions of this paper is threefold. Firstly, to provide experimental validation of the full modified kinematic control scheme presented in [11]. Secondly, to compare by simulation and experiments several kinematic control
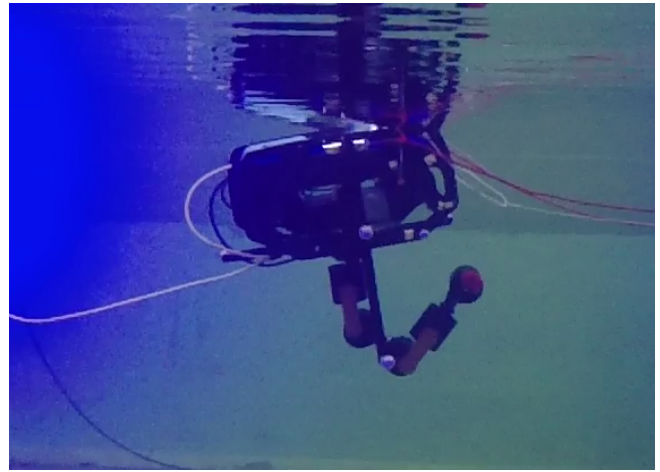
Fig. 1: The underwater vehicle-manipulator system (BlueROV2 [34] and SeaArm [35]) applied in the presented work.

schemes for stabilizing an UVMS end-effector. Thirdly, to present stability analysis for the kinematic control schemes and analyze the effect of the assumption of perfect velocity tracking. The kinematic control schemes discussed in this paper focuses on reducing end-effector position error. Naturally, the UVMS body position error and manipulator joint angle errors become less important, as it is ultimately the end-effector position accuracy that determines the tracking performance. In a real case scenario, however, both of the former errors are at least equally important, due to the risk of collision, entanglement with the tether, and so on. In this paper, a simple, constant position scenario is investigated, where both the underwater vehicle body and the end-effector have constant setpoints. Additionally, an external force is induced on the vehicle as a slowly time-varying disturbance acting on the system. This force simulates the effect of an underwater current, which is the main unknown disturbance in deep water operations. The experiments show basic performance and shed light upon some fundamental strengths and weaknesses of the three different control schemes. Experiments were conducted in the Marine Cybernetics Laboratory (MC-lab), a lab testing facility at the Norwegian University of Science and Technology (NTNU) in Trondheim, Norway. The system used for testing is shown in Fig. 1.

The paper is organized as follows. Section 2 gives a brief introduction to the system description, while Section 3 presents the equations of motion for the UVMS. Section 4 introduces the various control schemes for controlling the UVMS. Stability analysis of the three different kinematic control schemes is presented in Section 5. Section 6 provides information on the underwater vehicle, the manipulator and the communication interface, in addition to describing the testing facility, the testing procedure and the results from the experimental testing. Finally, Section 7 discusses the results and Section 8 holds the concluding remarks.

2. System Description

The UVMS considered in this paper is a small, lightweight UVMS based on combining the BlueROV2 [34] with the SeaArm manipulator arm [35] depicted in Fig. 1. The chosen setup for the manipulator arm is three degrees of freedom (3 DOF). Due to the low number of DOF for the manipulator arm, and the fact that the system is chosen to be slightly positively buoyant for practical reasons during the experimental testing phase, only x- and y-position is controlled. Sections 6.2-6.3 give a more detailed description of the manipulator arm and the BlueROV2 underwater vehicle.

3. Equations of Motion

The UVMS model is based on [21], where the state of the UVMS base is described by the position $\boldsymbol{\eta} = [\boldsymbol{p}^T \ \boldsymbol{\theta}^T]^T$ and velocity $\boldsymbol{\nu} = [\boldsymbol{v}^T \ \boldsymbol{\omega}^T]$. Here, $\boldsymbol{p} = [x, y, z]^T$ is the position and $\boldsymbol{\Theta} = [\phi, \theta, \psi]^T$ is the Euler angles of the vehicle's body frame expressed in the NED frame. Furthermore, $\boldsymbol{v} = [u, v, w]^T$ is the linear velocity and $\boldsymbol{\omega} = [p, q, r]^T$ is the angular velocity of the body frame expressed in the body frame. The manipulator state is described by the joint angles $\boldsymbol{q} = [q_1, q_2, q_3]^T$ and joint angular rates $\dot{\boldsymbol{q}} = [\dot{q}_1, \dot{q}_2, \dot{q}_3]$. The position and orientation of the end-effector is described by the end-effector position in the NED frame $\boldsymbol{p}_{ee} = [x_{ee}, y_{ee}, z_{ee}]^T$ and the end-effector Euler angles $\boldsymbol{\Theta}_{ee} = [\phi_{ee}, \theta_{ee}, \psi_{ee}]^T$.

The dynamic equations are not used here as the suggested control scheme requires no model knowledge. Hence, only the kinematic equations are considered. For a detailed description on the UVMS kinematics and dynamics, see [5], [7], [21], [36], [37]. The kinematic equations are given by [5]

$$\dot{\boldsymbol{\eta}} = \boldsymbol{J}_R(\boldsymbol{\eta})\boldsymbol{\nu} \qquad (1)$$

$$\dot{\boldsymbol{x}}_{ee} = \boldsymbol{J}_1(\boldsymbol{q})\dot{\boldsymbol{q}} + \boldsymbol{J}_2(\boldsymbol{\eta})\boldsymbol{\nu} = \boldsymbol{J}_e(\boldsymbol{q}, \boldsymbol{\eta})\boldsymbol{\zeta} \qquad (2)$$

where $\boldsymbol{\zeta} = [\dot{\boldsymbol{q}}^T \ \boldsymbol{\nu}^T]^T$ represents the velocity of both the UVMS body and the manipulator, $\boldsymbol{J}_R$ is the Jacobian for the UVMS base and $\boldsymbol{J}_e$ is the Jacobian relating the end-effector time derivative to $\boldsymbol{\zeta}$.

4. Control

The control scheme applied in the presented work consists of two parts. In this section, both parts of the control scheme are presented; the kinematic control scheme, which generates reference velocities, and the lower level sliding mode controller, used for velocity tracking. The structure of the control scheme can be seen in Fig. 2.

One of the strengths of the kinematic control approach is that it is possible to define several tasks for the system in a given order of priority, for which the lower priority tasks will not affect the higher priority tasks. This is handled by projecting the reference velocities of the lower priority tasks onto the null space of the reference velocities of the higher priority tasks. However, this relies on an assumption that the reference velocities are followed perfectly. As discussed,
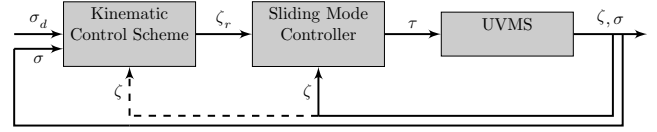
Fig. 2: Overview of the control system. The dashed line shows the extra feedback added in the FMKC scheme.

this is not always the case for the UVMS body, as velocity tracking is difficult when subjected to unknown, time-varying disturbances due to the large inertia of the UVMS body, in addition to the dynamics of the thrusters.

Three kinematic control approaches are implemented and compared, and will shed light on the weakness of assuming reference velocities are followed perfectly. Two of the control approaches are well known, and the third is the control approach proposed in [11]:

- Decoupled Kinematic Control (DKC): This kinematic control scheme reduce the problem to keeping the end-effector at a constant position with unknown UVMS body movement and keeping the UVMS body at a constant position, treating the two systems as decoupled from one another.
- Full Kinematic Control (FKC): This approach takes the whole system and its Jacobians into account, viewing the system as a kinematically redundant system with two tasks. The task with first priority is to keep the end-effector at a constant position and the second priority task is to keep the UVMS body at a constant position.
- Full Modified Kinematic Control (FMKC): The Full Modified Kinematic Control scheme is based on the control scheme proposed in [11], where a term taking the lower-level tracking error of the vehicle into account when generating desired velocities for the end-effector is added.

The output from the kinematic control schemes is reference velocities $\boldsymbol{\zeta}_r = [\boldsymbol{q}_r^T \ \boldsymbol{\nu}_r^T]^T$, which must be followed by a lower-level velocity controller. A sliding mode controller is chosen for the experiments, as in simulations in [11]. The reason for choosing the stated sliding mode control law for the experimental testing is that this controller does not require any knowledge of the dynamic model. The proposed kinematic control schemes, however, can be implemented with any velocity controller. Consequently, if a model-based controller showing good tracking performance in a real scenario is available, this can be used instead.

4.1 Sliding Mode Controller

The principle behind the sliding mode controller is to make the states of the system converge to a sliding manifold which has global exponential stability. In this paper, this manifold is chosen as

$$\boldsymbol{s} = \begin{bmatrix} \dot{\boldsymbol{q}}_r - \dot{\boldsymbol{q}} \\ \boldsymbol{\nu}_r - \boldsymbol{\nu} \end{bmatrix} + \boldsymbol{\Lambda} \int_0^t \begin{bmatrix} \dot{\boldsymbol{q}}_r - \dot{\boldsymbol{q}} \\ \boldsymbol{\nu}_r - \boldsymbol{\nu} \end{bmatrix} d\tau = \boldsymbol{0} \qquad (3)$$

where $\mathbf{\Lambda}$ is a gain matrix and $\boldsymbol{\nu}_r$ and $\dot{\boldsymbol{q}}_r$ are the reference velocities and angular velocities generated by the kinematic control scheme described in Section 4.2. This manifold is globally exponentially stable if $\mathbf{\Lambda} > 0$. The control law is given by [5]

$$\boldsymbol{\tau} = \boldsymbol{K}_D \boldsymbol{s} + \hat{\boldsymbol{g}}(\boldsymbol{q}, \boldsymbol{\Theta}_{nb}) + \boldsymbol{K}_S \text{sat}(\boldsymbol{s}, \varepsilon) \tag{4}$$

where $\boldsymbol{K}_D > 0$, $\boldsymbol{K}_S > 0$ are gain matrices and $\hat{\boldsymbol{g}}(\boldsymbol{q}, \boldsymbol{\Theta}_{nb})$ is an estimate of the restoring forces and torques. However, as the UVMS in experiments is positively buoyant and floating in the surface, $\hat{\boldsymbol{g}}(\boldsymbol{q}, \boldsymbol{\Theta}_{nb})$ can be omitted for the experiments in this paper. The reason for choosing the saturation function $\text{sat}(\boldsymbol{s}, \varepsilon)$ instead of a signum function is to avoid chattering, as discussed in [30].

4.2 Kinematic Control

Kinematic control is based on taking advantage of the kinematic relations in the system, described by tasks and their Jacobian, i.e., (1) and (2), and simplified versions of these [5]. The task of finding system state velocities given desired end-effector velocities is a much more tractable problem than solving the inverse relations for a given desired end-effector position. A task χ may be described through the generic variable

$$\boldsymbol{\sigma}_\chi = \boldsymbol{\sigma}_\chi(\boldsymbol{q}, \boldsymbol{\eta}) \in \mathbb{R}^m \tag{5}$$

and its Jacobian

$$\dot{\boldsymbol{\sigma}}_\chi = \boldsymbol{J}_\chi(\boldsymbol{q}, \boldsymbol{\eta})\boldsymbol{\zeta} \tag{6}$$

The two tasks considered in this paper are end-effector x- and y-position (2 DOF) and UVMS base x- and y-position and heading ψ (3 DOF). This could be extended to full 6 DOF end-effector configuration, but because of the simple 3 DOF manipulator arm, only the end-effector position (x_{ee}, y_{ee}) position is controlled. Consequently, we define the end-effector position as a task by the variable σ, written as

$$\boldsymbol{\sigma}_1 = [x_{ee}, y_{ee}]^T \tag{7}$$

The subscript refers to the priority of the task. The Jacobian for $\boldsymbol{\sigma}_1$ will vary with each control scheme, and will be specified. Furthermore, the task of controlling the vehicle position and heading (x, y, ψ) and the Jacobian of the task parameter is given as

$$\boldsymbol{\sigma}_2 = [x, y, \psi]^T \tag{8}$$

$$\boldsymbol{J}_2 = \begin{bmatrix} \boldsymbol{R}^n_{b_{1:2 \times 1:3}} & \boldsymbol{0}_{2 \times 6} \\ \boldsymbol{0}_{1 \times 3} & \boldsymbol{T}_{3 \times 1:3} & \boldsymbol{0}_{1 \times 3} \end{bmatrix} \tag{9}$$

where $\boldsymbol{R}^n_{b_{1:2 \times 1:3}}$ is the first and second row of the rotation matrix from body to the world frame, $\boldsymbol{R}^n_b \in \mathbb{R}^{3x3}$. Furthermore, $\boldsymbol{T}_{3 \times 1:3}$ is the third row of the transformation from angular velocity to Euler angle rates, $\boldsymbol{T}$, described in

detail in [36]. The reference velocities are calculated using the weighted pseudo inverse

$$\boldsymbol{\zeta}_r = \boldsymbol{J}^\dagger_{\chi, \boldsymbol{W}_\chi}(\boldsymbol{q}, \boldsymbol{\eta})\dot{\boldsymbol{\sigma}}_{\chi, r} \tag{10}$$

The weighted pseudo inverse is given as

$$\boldsymbol{J}^\dagger_{\chi, \boldsymbol{W}_\chi} = \boldsymbol{W}^{-1}_\chi \boldsymbol{J}^T_\chi \left(\boldsymbol{J}_\chi \boldsymbol{W}^{-1}_\chi \boldsymbol{J}^T_\chi \right)^{-1} \tag{11}$$

where the notation $(\boldsymbol{q}, \boldsymbol{\eta})$ is omitted for enhanced readability. The variable $\boldsymbol{W}_\chi$ is a weighting matrix and $\dot{\boldsymbol{\sigma}}_{\chi, r}$ corresponds to the reference task velocity. According to [5], the reference task velocity can be chosen as a function of the task error as $\dot{\boldsymbol{\sigma}}_{\chi, r} = \boldsymbol{k}_\chi \tilde{\boldsymbol{\sigma}}_\chi$, and will be used as a feedback to increase convergence towards the desired values, where $\boldsymbol{k}_\chi$ is a gain matrix. Naturally, the task error is found as $\tilde{\boldsymbol{\sigma}}_\chi = \boldsymbol{\sigma}_{\chi, d} - \boldsymbol{\sigma}_\chi$, where $\boldsymbol{\sigma}_{\chi, d}$ is the desired values for task χ. For the two-task approach, the Singularity Robust Task Priority Redundancy Resolution Technique [5], [12] will be used, where the reference velocities associated with the second task are projected onto the null space of the reference velocities of the primary task, similar to what was done in [5] and [38]. The set points are stationary, which implies that the desired task velocity is a function of the task error. The expression for the reference velocities $\boldsymbol{\zeta}_r$ is given by the equation

$$\boldsymbol{\zeta}_r = \boldsymbol{J}^\dagger_{1, \boldsymbol{W}_1} \boldsymbol{k}_1 \tilde{\boldsymbol{\sigma}}_1 + \boldsymbol{Z}_1 \boldsymbol{J}^\dagger_{2, \boldsymbol{W}_2} \boldsymbol{k}_2 \tilde{\boldsymbol{\sigma}}_2 \tag{12}$$

where $\boldsymbol{k}_1, \boldsymbol{k}_2 > 0$ are gain matrices and the parameter $\boldsymbol{Z}_1$ is calculated as

$$\boldsymbol{Z}_1 = \left(\boldsymbol{I}_{9x9} - \boldsymbol{J}^\dagger_{1, \boldsymbol{W}_1} \boldsymbol{J}_1 \right) \tag{13}$$

The three kinematic control schemes will be presented in the following.

4.3 Decoupled Kinematic Control (DKC)

To describe that all movement of the end-effector should be done by the manipulator arm only, the Jacobian for the end-effector in the decoupled kinematic control scheme J_1 is given by

$$\boldsymbol{J}_1 = \begin{bmatrix} \boldsymbol{J}_{man} & \boldsymbol{0}_{2x6} \end{bmatrix} \tag{14}$$

where $\boldsymbol{J}_{man} \in \mathbb{R}^{2 \times 3}$ is is the Jacobian of the manipulator arm. The Jacobian for the interconnected system, $\boldsymbol{J}_{UVMS}$, is described in detail in [5], and is given by

$$\boldsymbol{J}_{UVMS} = [\boldsymbol{J}_{man},$$

$$\boldsymbol{R}^I_b, - \left(\boldsymbol{S}(\boldsymbol{R}^n_b \boldsymbol{r}^b_{b0}) + \boldsymbol{S}(\boldsymbol{R}^n_0 \boldsymbol{\eta}^0_{0,ee}) \right) \boldsymbol{R}^I_b] \tag{15}$$

where $\boldsymbol{S}(\cdot)$ is the cross-product operator, $\boldsymbol{r}^b_{b0}$ is the vector from the origin of the body coordinate frame to the origin of the manipulator base coordinate frame, $\boldsymbol{R}^n_0$ is the rotation matrix from the world frame to the manipulator base frame, and $\boldsymbol{\eta}^0_{0,ee}$ is the vector from the manipulator base origin to the end-effector. Note that as the end-effector task is chosen as in (7), only the two first rows of $\boldsymbol{J}_{UVMS}$ are applied.

4.4 Full Kinematic Control (FKC)

For the full kinematic control approach, the Jacobian for the end-effector J_1 is described by the full Jacobian in (15) as

$$J_1 = J_{UVMS} \tag{16}$$

As the name suggests, the FKC scheme incorporates velocities for both the vehicle and the manipulator, which leads to a full consideration of the UVMS motions. The FKC scheme also assumes that the reference velocities are tracked perfectly. This is not the case for the DKC scheme, since it treats the vehicle body motions as a disturbance.

4.5 Full Modified Kinematic Control (FMKC)

In the suggested full modified kinematic control (FMKC) approach, the task Jacobian is similar to (16). However, (12) is now modified to take velocity tracking error into account by adding the term $W_e(\zeta_r - \zeta)$, where W_e is a weighting matrix, as follows

$$\zeta_r = J_{1,W_1}^{\dagger}(k_1 \tilde{\sigma}_1 + W_e(\zeta_r - \zeta)) + Z_1 J_{2,W_2}^{\dagger} k_2 \tilde{\sigma}_2 \tag{17}$$

which leads to the following expression for ζ_r:

$$\zeta_r = \mathbf{S}^{-1} \left(J_{1,W_1}^{\dagger}(k_1 \tilde{\sigma}_1 - W_e \zeta) \right.$$
$$\left. + Z_1 J_{2,W_2}^{\dagger} k_2 \tilde{\sigma}_2 \right) \tag{18}$$

where

$$\mathbf{S} = \left(I_{9x9} - J_{1,W_1}^{\dagger} W_e \right)$$

The velocity tracking error $\tilde{\zeta} = \zeta_d - \zeta$ is mainly meant to aid the manipulator in reaching desired end-effector position when disturbances such as ocean currents are present, which is when the vehicle is having the hardest time reaching its desired position. By assuming that ocean currents are irrotational, only the velocity components of the vehicle in the x- and y-direction are accounted for. The natural choice for W_e is J_{UVMS}, in which the velocity tracking errors are transformed into end-effector velocity and added to the desired end-effector velocity. However, this will yield a reinforcing loop, and $\mathbf{S}$ will be singular, thus not invertible. Clearly this is not an option, but there are other ways of taking tracking error into account; by choosing the weighting matrix in $J_{1,W_1}^{\dagger}$ such that only the manipulator arm is activated to achieve desired end-effector velocity, and only adding underwater vehicle base velocity tracking error, a decoupling is introduced, avoiding a reinforcing loop and singularities. This is done by choosing either $W_1 = \text{diag}([\mathbf{1}_{1xn}, \infty_{1x6}])$ or J_1 like in (14) and $W_e = \begin{bmatrix} \mathbf{0}_{2xn} & J_{UVMS}^{4:9} \end{bmatrix}$, where $n = 3$ is the number of joints of the manipulator arm that are controlled and $\mathbf{J}_{UVMS}^{4:9}$ contains the last 6 columns in $\mathbf{J}_{UVMS}$.

It is important to note that the Jacobian can be inverted, which will be considered in the following. When the matrices are chosen as described above, $J_{1,W_1}^{\dagger}$ will, for any number of joints n, have the structure

$$J_{1,W_1}^{\dagger} = \begin{bmatrix} \mathbf{G}_{n \times 3} \\ \mathbf{0}_{6 \times 3} \end{bmatrix} \tag{19}$$

which results in

$$\mathbf{S} = \begin{bmatrix} \mathbf{I}_{n \times n} & \mathbf{C}_{n \times 6} \\ \mathbf{0}_{6 \times n} & \mathbf{I}_{6 \times 6} \end{bmatrix} \tag{20}$$

where $\mathbf{G}$ and $\mathbf{C}$ are matrices dependent on the states and properties of the system. To show that $\mathbf{S}$ will always be invertible, consider the block wise matrix inversion formula given by

$$\begin{bmatrix} \mathbf{A} & \mathbf{B} \\ \mathbf{C} & \mathbf{D} \end{bmatrix}^{-1} = \begin{bmatrix} \mathbf{A}^{-1} + \mathbf{A}^{-1}\mathbf{B}(\mathbf{D} - \mathbf{C}\mathbf{A}^{-1}\mathbf{B})^{-1}\mathbf{C}\mathbf{A}^{-1} \\ -(\mathbf{D} - \mathbf{C}\mathbf{A}^{-1}\mathbf{B})^{-1}\mathbf{C}\mathbf{A}^{-1} \end{bmatrix}$$
$$\begin{bmatrix} -\mathbf{A}^{-1}\mathbf{B}(\mathbf{D} - \mathbf{C}\mathbf{A}^{-1}\mathbf{B})^{-1} \\ (\mathbf{D} - \mathbf{C}\mathbf{A}^{-1}\mathbf{B})^{-1} \end{bmatrix} \tag{21}$$

In this case, $\mathbf{A} = \mathbf{I}_{n \times n}$, $\mathbf{B} = \mathbf{C}_{n \times 6}$, $\mathbf{C} = \mathbf{0}_{6 \times n}$ and $\mathbf{D} = \mathbf{I}_{6 \times 6}$ which yields

$$\mathbf{S}^{-1} = \begin{bmatrix} \mathbf{I}_{n \times n} & -\mathbf{C}_{6 \times n} \\ \mathbf{0}_{n \times 6} & \mathbf{I}_{6 \times 6} \end{bmatrix} \tag{22}$$

Thus, $\mathbf{S}$ will be invertible, regardless of the values of system states and properties.

5. STABILITY ANALYSIS

This section aims to study the stability properties for kinematic control schemes of the DKC, FKC and FMKC in the sense of Lyapunov stability. The task at hand is denoted *equality task*, which means that the desired end-effector and UVMS body position is equal to a single value, as opposed to *inequality tasks* and *set-based tasks*, that allow for the end-effector and UVMS body positions to satisfy inequalities or to remain within a set of values, respectively [38]. The assumption that desired joint velocities are tracked perfectly by the system is used, and is common in closed loop inverse kinematics [39]. The assumption is valid in simulations, but may also be valid in physical systems. In general, the vehicle dynamics are slow, which implies that the UVMS body is unable to track references perfectly. This is not the case for the manipulator joints, which often has a low inertia, in addition to accurate encoders to determine joint angles. This goes hand in hand with the DKC and FMKC methods, which both make use of the vehicle's inability to follow references perfectly, but also works for the FKC method, which assumes that references are followed perfectly by design, typically at the expense of larger task errors.

In order to study the stability properties of the kinematic control schemes, it is of interest to investigate how the task errors behave. Similar to [38] and [39], the following Lyapunov function candidate is chosen for all three kinematic control schemes

$$V = \frac{1}{2} \tilde{\sigma}_\chi^T \tilde{\sigma}_\chi \tag{23}$$

The time derivative is found as

$$\dot{V} = \tilde{\boldsymbol{\sigma}}_\chi^T \dot{\tilde{\boldsymbol{\sigma}}}_\chi \tag{24}$$

Inserting $\tilde{\boldsymbol{\sigma}}_\chi = \boldsymbol{\sigma}_{\chi,d} - \boldsymbol{\sigma}_\chi$ into (24) and assuming perfect velocity tracking yields

$$\dot{V} = \tilde{\boldsymbol{\sigma}}_\chi^T (\dot{\boldsymbol{\sigma}}_{\chi,d} - \dot{\boldsymbol{\sigma}}_\chi) = -\tilde{\boldsymbol{\sigma}}_\chi^T \boldsymbol{J}_\chi \boldsymbol{\zeta}_r \tag{25}$$

The two tasks considered are tracking reference velocities for the manipulator and the vehicle in the Singularity Robust Task Priority Redundancy Resolution framework. By applying the reference velocities for both the manipulator and the vehicle in (12), it follows that (25) now becomes

$$\dot{V} = -\tilde{\boldsymbol{\sigma}}_1^T \boldsymbol{J}_1 \boldsymbol{\zeta}_{1,r} - \tilde{\boldsymbol{\sigma}}_2^T \boldsymbol{J}_2 \boldsymbol{Z}_1 \boldsymbol{\zeta}_{r,2} \tag{26}$$

where $\zeta_{r,1}$ and $\zeta_{r,2}$ correspond to the generated reference velocities for the manipulator joints and the vehicle, respectively. Furthermore, $\boldsymbol{Z}_1$ projects the reference velocities of the lower priority task 2 onto the null space of the reference velocities of priority task 1. Stability of each individual kinematic control scheme will now be studied more closely.

5.1 Stability of Decoupled Kinematic Control

For the DKC scheme, inserting (12) into (26) yields

$$\dot{V} = -\tilde{\boldsymbol{\sigma}}_1^T \boldsymbol{J}_1 (\boldsymbol{J}_{1,W_1}^\dagger \boldsymbol{k}_1) \tilde{\boldsymbol{\sigma}}_1$$
$$-\tilde{\boldsymbol{\sigma}}_2^T \boldsymbol{J}_2 \boldsymbol{Z}_1 (\boldsymbol{J}_{2,W_2}^\dagger \boldsymbol{k}_2) \tilde{\boldsymbol{\sigma}}_2 \tag{27}$$

Applying the pseudoinverse presented in (11) to (27) gives

$$\dot{V} = -\tilde{\boldsymbol{\sigma}}_1^T \left(\boldsymbol{J}_1 \boldsymbol{W}_1^{-1} \boldsymbol{J}_1^T (\boldsymbol{J}_1 \boldsymbol{W}_1^{-1} \boldsymbol{J}_1^T)^{-1} \right) \boldsymbol{k}_1 \tilde{\boldsymbol{\sigma}}_1$$
$$-\tilde{\boldsymbol{\sigma}}_2^T \left(\boldsymbol{J}_2 \boldsymbol{Z}_1 \boldsymbol{W}_2^{-1} \boldsymbol{J}_2^T (\boldsymbol{J}_2 \boldsymbol{W}_2^{-1} \boldsymbol{J}_2^T)^{-1} \right) \boldsymbol{k}_2 \tilde{\boldsymbol{\sigma}}_2 \tag{28}$$

Given that the system is far away from singularities so that $\boldsymbol{J}_1 \boldsymbol{W}_1^{-1} \boldsymbol{J}_1^T (\boldsymbol{J}_1 \boldsymbol{W}_1^{-1} \boldsymbol{J}_1^T)^{-1}$ and $\boldsymbol{J}_2 \boldsymbol{W}_2^{-1} \boldsymbol{J}_2^T (\boldsymbol{J}_2 \boldsymbol{Z}_1 \boldsymbol{W}_2^{-1} \boldsymbol{J}_2^T)^{-1}$ are well-defined, it follows that the time derivative of the Lyapunov function becomes

$$\dot{V} = -\tilde{\boldsymbol{\sigma}}_1^T \boldsymbol{k}_1 \tilde{\boldsymbol{\sigma}}_1 - \tilde{\boldsymbol{\sigma}}_2^T \boldsymbol{k}_2 \tilde{\boldsymbol{\sigma}}_2 \tag{29}$$

By consulting [5] and (26) in [39], if the Jacobians can be set on this form and satisfy the equality condition

$$\rho(\boldsymbol{J}_1^T) + \rho(\boldsymbol{J}_2^T) = \rho([\boldsymbol{J}_1^T \, \boldsymbol{J}_2^T]) \tag{30}$$

the two tasks are *independent*, where $\rho(\cdot)$ denotes the *rank*-operator. Worth to note, this can only be guaranteed as long as singularities are avoided, which implies that $\boldsymbol{Z}_1$ is positive definite. The same argumentation also holds for the FKC and the FMKC schemes. The system in (29) can be rewritten as

$$\dot{V} = -\tilde{\boldsymbol{\sigma}}^T \boldsymbol{K} \tilde{\boldsymbol{\sigma}} \tag{31}$$

with $\tilde{\boldsymbol{\sigma}} = [\tilde{\boldsymbol{\sigma}}_1 \, \tilde{\boldsymbol{\sigma}}_2]$ and $\boldsymbol{K} = diag(\boldsymbol{k}_1, \boldsymbol{k}_2)$. By carrying out the calculation in (30), it follows that the two tasks are independent and the gains matrix $\boldsymbol{K}$ is positive definite by choosing the gains $\boldsymbol{k}_1, \, \boldsymbol{k}_2 > \boldsymbol{0}$. It then follows that $\dot{V}$ is

negative definite. Hence, the DKC scheme makes it so that the task errors $\tilde{\boldsymbol{\sigma}} = [\tilde{\boldsymbol{\sigma}}_1 \, \tilde{\boldsymbol{\sigma}}_2]$ converge to zero asymptotically, i.e. $\tilde{\boldsymbol{\sigma}} = \boldsymbol{0}$ is asymptotically stable. Furthermore, if $\boldsymbol{q}$ belongs to a compact set, similar to [38], $\tilde{\boldsymbol{\sigma}} = \boldsymbol{0}$ is exponentially stable.

5.2 Stability of Full Kinematic Control

The difference between the DKC and the FKC scheme is that FKC uses a different Jacobian $\boldsymbol{J}_1$ for the manipulator. However, by the same argumentation as for the DKC scheme, the task errors in the FKC scheme $\tilde{\boldsymbol{\sigma}} = \boldsymbol{0}$ is asymptotically stable. Furthermore, if $\boldsymbol{q}$ belongs to a compact set, $\tilde{\boldsymbol{\sigma}} = \boldsymbol{0}$ is exponentially stable.

5.3 Stability of Full Modified Kinematic Control

In the FMKC scheme, the Jacobians are similar to the Jacobians of the FKC method, but the velocity reference is now given by (18). Inserting this into (25) yields

$$\dot{V} = -\tilde{\boldsymbol{\sigma}}_1^T \boldsymbol{J}_1 \left(\boldsymbol{S}^{-1} \boldsymbol{J}_{1,W_1}^\dagger \boldsymbol{k}_1 \tilde{\boldsymbol{\sigma}}_1 - \boldsymbol{S}^{-1} \boldsymbol{W}_e \boldsymbol{\zeta} \right)$$
$$- \tilde{\boldsymbol{\sigma}}_2^T \boldsymbol{J}_2 \boldsymbol{S}^{-1} \boldsymbol{Z}_1 \boldsymbol{J}_{2,W_2}^\dagger \boldsymbol{k}_2 \tilde{\boldsymbol{\sigma}}_2 \tag{32}$$

By design, $\boldsymbol{S}^{-1}$ is positive definite, and by the argument in Section 5.1, $\boldsymbol{Z}_1$ is positive definite. Therefore, $\boldsymbol{S}^{-1}$ and $\boldsymbol{Z}_1$ are left out for increased readability, as it does not affect the stability properties of the system. Recognizing that $\boldsymbol{\zeta} = \boldsymbol{\zeta}_r - \tilde{\boldsymbol{\zeta}}$ and that the reference velocity can be written as the Jacobian times the time derivative of the task error as $\tilde{\boldsymbol{\zeta}} = \boldsymbol{J}_{\chi,W_\chi}^\dagger \dot{\tilde{\boldsymbol{\sigma}}}_\chi$ yields

$$\boldsymbol{\zeta} = \boldsymbol{J}_{\chi,W_\chi}^\dagger \dot{\boldsymbol{\sigma}}_{\chi,r} - \boldsymbol{J}_{\chi,W_\chi}^\dagger \dot{\tilde{\boldsymbol{\sigma}}}_\chi \tag{33}$$

Inserting for $\dot{\boldsymbol{\sigma}}_{\chi,r} = \boldsymbol{k}_\chi \tilde{\boldsymbol{\sigma}}_\chi$ and $\dot{\tilde{\boldsymbol{\sigma}}}_\chi = \dot{\boldsymbol{\sigma}}_{\chi,d} - \dot{\boldsymbol{\sigma}}_\chi$, it follows that (33) can be reduced to

$$\boldsymbol{\zeta} = 2\boldsymbol{J}_{\chi,W_\chi}^\dagger \boldsymbol{k}_\chi \tilde{\boldsymbol{\sigma}}_\chi \tag{34}$$

With $\boldsymbol{W}_e = [\boldsymbol{0}_{2\times6} \, \boldsymbol{J}_{UVMS}]$, $\boldsymbol{J}_1$ and $\boldsymbol{J}_2$ as defined previously and inserting (33) into (32), it follows that (32) is reduced to

$$\dot{V} = -\tilde{\boldsymbol{\sigma}}_1^T \boldsymbol{k}_1 \tilde{\boldsymbol{\sigma}}_1 - \tilde{\boldsymbol{\sigma}}_2^T \boldsymbol{k}_2 \tilde{\boldsymbol{\sigma}}_2$$
$$+ 2\tilde{\boldsymbol{\sigma}}_1^T [\boldsymbol{0}_{2\times6} \, \boldsymbol{J}_{UVMS}^{4:9}] \boldsymbol{J}_{2,W_2}^\dagger \boldsymbol{k}_2 \tilde{\boldsymbol{\sigma}}_2 \tag{35}$$

Note that only the first two rows of $\boldsymbol{J}_{UVMS}$ are used, as previously stated. This means that only velocity error in x- and y-direction of the vehicle are used when making the end-effector compensate for the vehicle body velocity tracking error. Carrying out the calculation of (35), the time derivative becomes

$$\dot{V} = -\tilde{\boldsymbol{\sigma}}_1^T \boldsymbol{k}_1 \tilde{\boldsymbol{\sigma}}_1 - \tilde{\boldsymbol{\sigma}}_2^T \boldsymbol{k}_2 \tilde{\boldsymbol{\sigma}}_2 + 2\tilde{\boldsymbol{\sigma}}_1 \boldsymbol{k}_3 \tilde{\boldsymbol{\sigma}}_2 \tag{36}$$

where the gain $\boldsymbol{k}_3$ contains the two first diagonal elements of $\boldsymbol{k}_2$, and is written as

$$\boldsymbol{k}_3 = \begin{bmatrix} \boldsymbol{k}_{2,11} & 0 & 0 \\ 0 & \boldsymbol{k}_{2,22} & 0 \end{bmatrix} \tag{37}$$

By proceeding with the calculation and letting the combined task errors be written as $\tilde{\boldsymbol{\sigma}} = [\tilde{\boldsymbol{\sigma}}_1 \; \tilde{\boldsymbol{\sigma}}_2]$, it is evident that (36) can be reduced to

$$\dot{V} = -\tilde{\boldsymbol{\sigma}}^T \boldsymbol{P} \tilde{\boldsymbol{\sigma}} \tag{38}$$

The matrix $\boldsymbol{P}$ is found as

$$\boldsymbol{P} = \begin{bmatrix} \boldsymbol{k}_{1,11} & 0 & 2\boldsymbol{k}_{2,11} & 0 & 0 \\ 0 & \boldsymbol{k}_{1,22} & 0 & 2\boldsymbol{k}_{2,22} & 0 \\ 0 & 0 & \boldsymbol{k}_{2,11} & 0 & 0 \\ 0 & 0 & 0 & \boldsymbol{k}_{2,22} & 0 \\ 0 & 0 & 0 & 0 & \boldsymbol{k}_{2,33} \end{bmatrix} \tag{39}$$

In order for $\boldsymbol{P}$ to be positive definite, it is required that all leading principle minors of $\boldsymbol{P}$ are positive definite. This is easy to obtain by choosing all elements in $\boldsymbol{k}_1, \boldsymbol{k}_2 > 0$. It follows that $\boldsymbol{P}$ is positive definite, which implies that $\dot{V}$ is negative definite. Hence, the origin of error tasks $\tilde{\boldsymbol{\sigma}} = \boldsymbol{0}$ converges to zero asymptotically. Finally, just as for the DKC and the FKC schemes, if $\boldsymbol{q}$ belongs to a compact set, $\tilde{\boldsymbol{\sigma}} = \boldsymbol{0}$ is exponentially stable [39].

Worth noticing is that the stability properties only hold locally for all possible states of $\boldsymbol{q}$ due to the existence of singularities. The assumption that a manipulator arm is able to track references perfectly may not be completely true and needs to be confirmed experimentally. However, due to the low inertia of small electric manipulator arms, such manipulators may be able to track references almost perfectly, in which case the stability results should hold. The fact that reference velocities are not tracked perfectly by an UVMS body implies that the task error of the vehicle position may be further analyzed with the interconnected control system, e.g., by cascaded systems theory [40]. This demands a comprehensive study on its own and is not further investigated here, as the main interest is the positioning capabilities of the manipulator arm and its end-effector.

6. EXPERIMENTAL TESTING AND RESULTS

This section introduces the manipulator arm and the underwater vehicle used in the experimental validation of the kinematic control schemes, the test basin located in the MC-lab at NTNU, the equipment and the experimental testing procedure. Finally, the results from the experiments are presented.

6.1 Marine Cybernetics Laboratory

The Marine Cybernetics Laboratory (MC-lab) at NTNU in Trondheim has been used as the test-facility, a small tank of size L x B x D = 40m x 6.45m x 1.5m. Six Oqus cameras and the Qualisys Track Manager (QTM) software together constitute a local underwater positioning system based on optical tracking. Lights emitted by the cameras are reflected by a set of markers that define a trackable object. This reflected light is captured by the cameras, and position and orientation estimates are available at a rate up to 100 Hz, with an accuracy of less than a centimeter. Readers are advised to visit [41] for more information.

TABLE I: Denvit-Hartenberg Parameters.

i	α_{i-1} [rad]	a_{i-1} [mm]	d_i [mm]	θ_i [rad]
1	0	0	55.3	θ_1
2	$-\pi/2$	0	0	$-\pi/2$
3	0	142.4	42.1	$\theta_2 - \pi/2$
4	$\pi/2$	142.4	0	$-\pi/2$
5	$-\pi/2$	0	13	$\theta_3 + \pi$
6	$\pi/2$	0	42.1	$\pi/2$
7	0	0	-139.6	$\theta_4 + \pi/2$
8	0	101	-59.6	0

6.2 Manipulator Arm

All information related to the manipulator arm is presented in [35], and the following may be viewed as a small summary. The manipulator is built completely modular with identical modules, making it straightforward to add or remove modules for altering the number of degrees of freedom. Each module contains an electric servo that provides torque about the joint axis. All of the modules are sealed with an o-ring lid, and are connected by hollow plates of stainless steel, which provide a waterproof environment for electronics and cables. The manipulator is 4 DOF, operating at 12 V and with a maximum reach of approximately 580 mm. The manipulator can be seen in Fig. 4, and the Denavit-Hartenberg (DH) convention parameters describing the reference frames to the links of the manipulator are given in Tab. I.

6.3 BlueROV2

The vehicle used in the experimental work is a BlueROV2. It has the size L x W x H = 457 x 338 x 254 [mm], and is an observation class ROV equipped with four horizontally and two vertically aligned T-200 thrusters, allowing it to move freely in surge, sway, heave and yaw. It weighs about 11kg and is slightly positively buoyant in water, with a maximum forward speed of approximately 1.5 m/s. A Raspberry Pi 3 (RPi3) communicates with all on-board devices, and is also used for communicating with the topside computer through an ethernet cable inside a neutrally buoyant tether. The tether

Fig. 3: The Marine Cybernetics Laboratory (MC-Lab) [41].
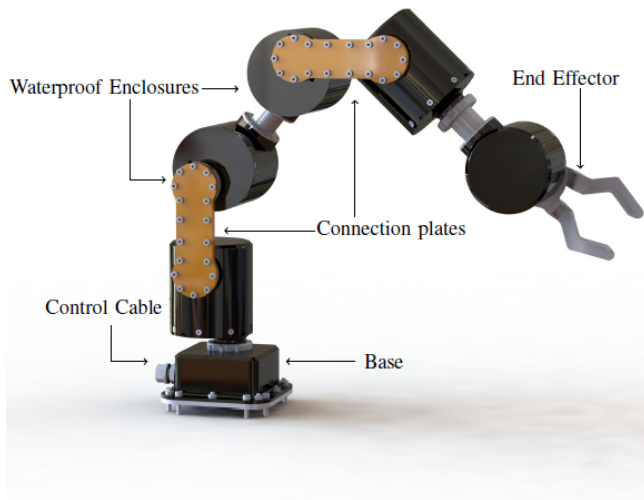
Fig. 4: A 3D model of the manipulator within the Solidworks 3D modelling environment [35].

Fig. 5: A 3D model of the BlueROV2 ROV and SeaArm manipulator arm within the Solidwork 3D modelling environment.

is used for receiving control commands and position data. The BlueROV2 ROV with the SeaArm manipulator arm is depicted in Figs. 1 and 5.

6.4 Interface and Communication

All communication from and to both the ROV and the manipulator takes place through the same type of communication interface, depicted in Fig. 6. A database stores the most recent information, acting as a a central server application that communicates through a publish (notify) and subscribe (register) protocol. This database is called the Mission Oriented Operating Suite Database (MOOSDB) [42]. Micro controllers allocate and route reference thrust values to the thrusters, and transmit generated manipulator commands to each respective joint angle servo.
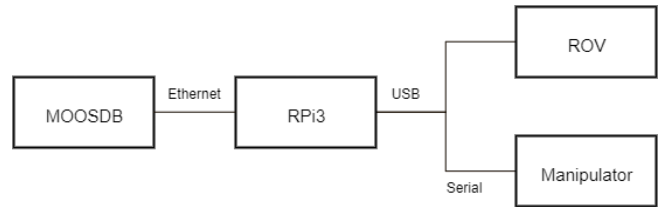
Fig. 6: Communication procedure and data flow.
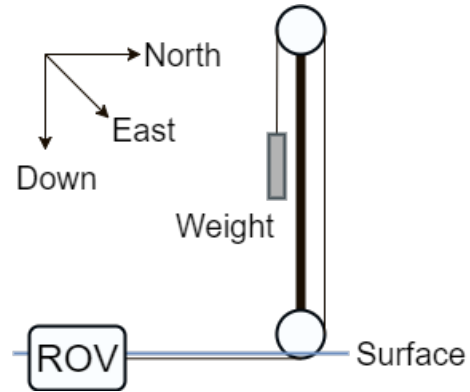
Fig. 7: The pulley system used to induce forces on the vehicle.

6.5 Experimental Testing Procedure

The overall goal of the testing is to verify the kinematic control schemes and the performance of the underwater vehicle-manipulator system when it comes to response, stability and accuracy. More specifically, the tests will show how well the manipulator is able to keep a fixed position during dynamic positioning of the ROV, while subjected to an unknown time-varying disturbance. The term dynamic positioning (DP) refers to the act of keeping a desired position in the horizontal plane (x, y) and heading (ψ). The experiment was set up as follows: Five QTM markers were placed on the ROV for position and attitude measurements, which was received at 50 Hz by the QTM. The manipulator was mounted under the ROV (see Figs. 1 and 5), and the position of the end-effector was measured based on the joint lengths and joint angles given by the servos. In order to simulate current forces on the vehicle, a pulley system was built. Loads could then be induced on the vehicle in the world frame, chosen as a local North-East-Down (NED) reference frame. The pulley system is depicted in Fig. 7. The rope that goes through the pulley was attached to the front of the vehicle close to its center of gravity (CG). By placing the vehicle so that the angle of the rope coincides with the local North, an unknown disturbance was induced on the system in the North direction. A disturbance of 0.53 kg (approximately 5 [N] force) was used in all of the experiments. Only the first three joints of the manipulator were operable, as the fourth joint does not contribute to lateral positioning and the fifth joint being the gripper. Each test case was concluded by the procedure given in the following.

1) Turn the power of the UVMS on
2) Set current position as the desired position
3) Run vehicle DP for 10 seconds
4) Run vehicle DP after adding the disturbance for 10 seconds
5) Run vehicle DP after removing the disturbance for 15 seconds
6) Turn the power of the UVMS off

For each of the control schemes, a total of ten experiments were conducted. After powering up in step 1, the vehicle waits for local position measurements from the QTM, and sets this position as the set point for experiment. In the third step, the vehicle performed DP at its initial position for about 10 seconds, and in step four, the load is "suddenly" induced on the vehicle, pulling the UVMS towards the pulley. After approximately 10 seconds, the experiment enters step five, where the load is removed. The vehicle is then given 15 seconds to stabilize. The procedure finally enters the phase six of the testing, where the UVMS is powered off.

6.6 Results

The tuning parameters for the experiments are shown in Tab. II. Note that the tuning parameters for the sliding mode controller only considers the six DOFs of the body, as the velocity control of each manipulator joint is handled internally in each servo. Furthermore, the tuning parameters are significantly lower than in simulation in [11], as the thruster commands in experiments are mapped from 0 (min) to 1 (max), instead of desired thrust in Newtons.

As described in Subsection 6.5, ten experiments were conducted for each kinematic control scheme. One of the runs for each control scheme (DKC, FKC, FMKC) shows the task errors $\tilde{\boldsymbol{\sigma}}_1 = [\tilde{x}_{ee}, \tilde{y}_{ee}]$ (end-effector position error) and $\tilde{\boldsymbol{\sigma}}_2 = [\tilde{x}, \tilde{y}, \tilde{\psi}]$ (underwater vehicle position and heading error), presented in Figs. 8 and 9, respectively. To illustrate the performance of the velocity controller, desired and real (measured) velocities from one of the experiments are shown for the manipulator arm in Fig. 10 and UVMS body in Fig. 11. As the lower-level sliding mode velocity controller is the same for all control schemes, only one example is sufficient to illustrate the vehicle velocity tracking performance for all three control schemes.

One of the runs for each of the DKC, FKC and FMKC schemes are shown in Figs. 12-14, respectively, and Fig. 15 show ten runs for each of these methods altogether. To
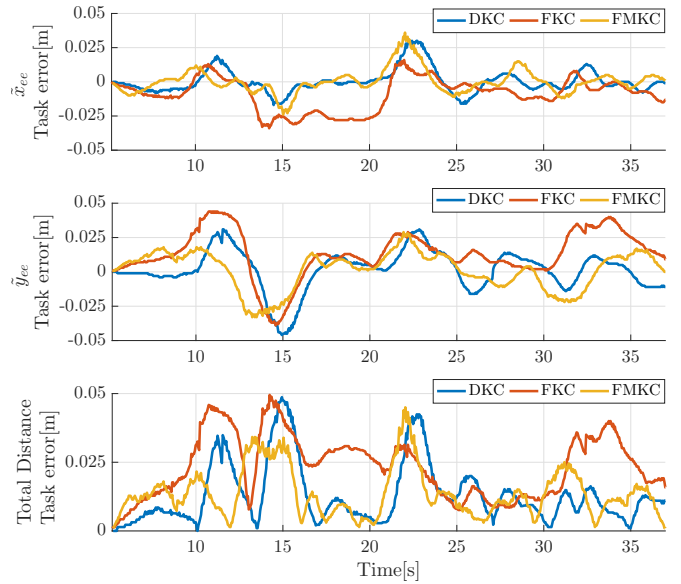
Fig. 8: A Sample run for each control scheme showing end-effector position error ($\tilde{\boldsymbol{\sigma}}_1$). The plots display the error w.r.t. time in x-direction ($\tilde{x}_{ee}$) in the top subplot, y-direction ($\tilde{y}_{ee}$) in the middle subplot and the total distance task error in the bottom subplot.

give an impression of the amount of stabilization needed for the manipulator arm, the unactuated end-effector position error, $\tilde{\boldsymbol{\sigma}}_{1\,UA}$, is also shown. The variable $\tilde{\boldsymbol{\sigma}}_{1\,UA}$ represents the end-effector position error if the manipulator arm had been completely static. This is typically the case for a 1 DOF manipulator arm, where the position control of the end-effector is solely dependent on the vehicle's position control capabilities. Furthermore, the standard deviation for the end-effector error for each control scheme is shown in Tab. III.

When comparing the results presented in Tab. III and Fig. 15, it is clear that the errors of DKC and FMKC are very similar, whereas the error for FKC is significantly larger. As the lower-level controller is the same for all three schemes, it can be assumed that the difference is in the kinematic control scheme. By taking another look at the example run in Fig. 8, it seems the most significant deviation between the control schemes is around $\text{Time} = 10s - 20s$ and $\text{Time} = 20s - 35s$. This time interval is in phase 4) and 5) of the testing procedure, respectively, where the externally applied disturbance is affecting the system. This is perhaps most easily notable in Figs. 12-14 at $\text{Time} \approx 10s$ and $\text{Time} \approx 20s$, and can also be seen in Fig. 11, where the tracking error of vehicle surge velocity u during the same time interval is larger than at other time instances. For the vehicle body, a larger deviation in velocity tracking can be expected in phases 4 and 5, where the unknown disturbance is induced on and removed from the system, respectively. Due to slow dynamics of the vehicle, the general assumption that reference velocities are followed perfectly in the kine-

TABLE II: Tuning parameter values for the experiments.

Parameter	Value
$\boldsymbol{\Lambda}_k$	$\mathbf{0}_{6\times 1}$
$\boldsymbol{K}_D$	$\text{diag}([\mathbf{0.6}_{1\times 3}, \mathbf{0.025}_{1\times 3}])$
$\boldsymbol{K}_S$	$\text{diag}([\mathbf{0.03}_{1\times 3}, \mathbf{1.25}_{1\times 3} \cdot 10^{-3}])$
$\boldsymbol{W}_1$	$\text{diag}([\mathbf{10}^6_{1\times 6}, \mathbf{1}_{1\times 3}])$
$\boldsymbol{W}_2$	$\text{diag}([\mathbf{10}^6_{1\times 6}, \mathbf{1}_{1\times 3}])$
$\boldsymbol{k}_1$	$1.5 \cdot \mathbf{I}_{2\times 1}$
$\boldsymbol{k}_2$	$0.5 \cdot \mathbf{I}_{3\times 1}$
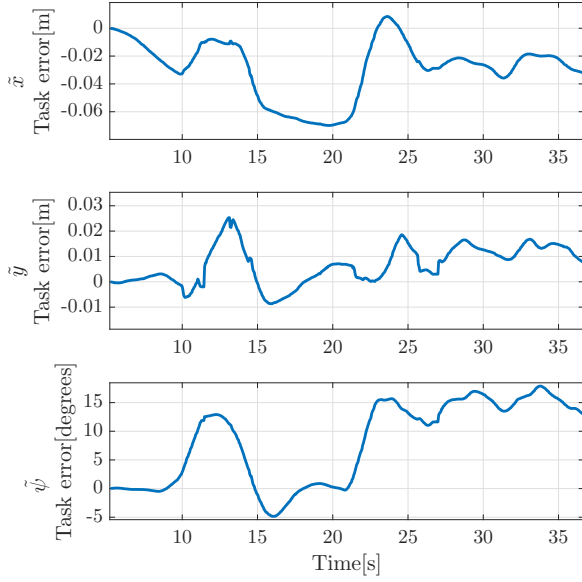
Fig. 9: A sample run showing underwater vehicle position and heading error ($\tilde{\boldsymbol{\sigma}}_2$). The plots display the error w.r.t. time in x-direction ($\tilde{x}$) in the top subplot, y-direction ($\tilde{y}$) in the middle subplot and heading ($\tilde{\psi}$) in the bottom subplot.

Fig. 10: Velocity tracking performance for the manipulator arm joints.

matic control framework becomes less valid. Furthermore, during phase 4 and 5, enhanced end-effector stabilization can be achieved if the motions of the vehicle body is treated as a disturbance, as is the case for the DKC scheme. This can also be attained if the tracking error is taken into account appropriately, which is what the FMKC scheme does. The incorporation of velocity tracking and the decoupling of manipulator and vehicle body is lacking in the FKC scheme, and hence, it does not achieve the same response as either DKC or FMKC. As mentioned in Section 4.4, FKC assumes that references are tracked perfectly. Conventionally, this is not the case, as the dynamics of the vehicle are slow and most certainly does not manage to track the reference perfectly. Therefore, it is better to decouple the system (DKC) or to incorporate the vehicle task velocity error (FMKC).

All three control schemes seem to have an error distribution that is diagonally spread from the lower left corner to the upper right corner of the xy-plane, both for $\tilde{\boldsymbol{\sigma}}_1$ and $\tilde{\boldsymbol{\sigma}}_{1\,UA}$. From Fig. 9 and Fig. 11 it is clear that both desired yaw angle and reference yaw rate of the UVMS body are not followed as desired. A possible explanation for this is a combination of deadband in the thrusters and a torque affecting the UVMS body from the tether. Deadband in one or more of the thrusters keep the vehicle from correcting for the offset, while a twist on the tether both drags and rotates the vehicle slightly. In order to measurement the behavior of the task errors, the Root Mean Square Error (RMSE) has been used. The RMSE over ten trials for each control scheme can be seen in Tab. IV.

The RMSE for DKC and FMKC are similar, whereas the

TABLE III: Task error standard deviations for the end-effector position in x and y direction for each control scheme, combined for all ten experiments.

Scheme	DKC	FKC	FMKC
$\tilde{\sigma}_{1,x_{ee}}$ [cm]	0.92	1.28	0.94
$\tilde{\sigma}_{1,y_{ee}}$ [cm]	1.39	1.76	1.36

RMSE for FKC is almost twice as large as the RMSE for DKC and FMKC. However, as it is impossible to run several control schemes at the same time, variation in environmental factors when testing each control scheme should also be considered. Even though efforts were made to make the environment as similar as possible between testing of each control scheme, variations in battery voltage, friction of the pulley-system, force from the tether, water motions and varying initial positions might affect performance.

The theoretical RMSE of the end-effector position if the manipulator arm was static, and thus not subjected to control, gives a good impression of the amount of stabilization necessary for the manipulator arm. Due to the choice of the task Jacobians and weight matrices in each control scheme, control of the UVMS body is identical for all control schemes, validating the claim that difference in UVMS body

TABLE IV: RMSE [cm] for each control scheme for the ten experimental trials.

Control Scheme	RMSE$_{\tilde{\boldsymbol{\sigma}}_1}$	RMSE$_{\tilde{\boldsymbol{\sigma}}_{1,UA}}$	$\frac{\text{RMSE}_{\tilde{\boldsymbol{\sigma}}_1}}{\text{RMSE}_{\tilde{\boldsymbol{\sigma}}_{1,FKC}}}$
DKC	1.66	7.64	0.61
FKC	2.73	7.23	1
FMKC	1.65	8.62	0.60
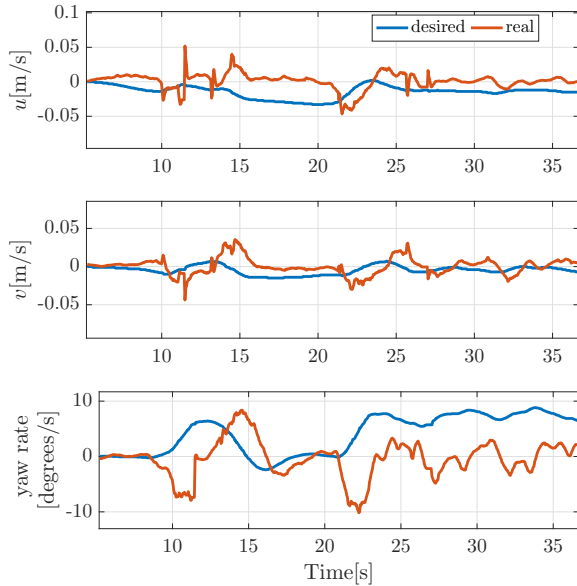
Fig. 11: Velocity tracking performance for the vehicle during DP.

Fig. 12: A sample run showing end-effector error in x and y direction and the total error distance w.r.t. time for the DKC method.

control performance is due to environmental variations. By studying the RMSE of the end-effector position in Tab. IV, it seems that due to changes in the environment, the UVMS body control was less accurate during testing of the FMKC scheme (RMSE around $1\,\mathrm{cm}$ larger). Thus the need for manipulator stabilization was more apparent during the test of FMKC. Furthermore, the ratios between RMSEs for the DKC control scheme in Tab. IV is similar to what was found in the simulation study in [11]. However, the performance of DKC and FMKC are more similar in experiments than in simulation and the differences in performance between the three schemes are smaller. A possible explanation can be extracted by studying Fig. 10. It is clear that there is a delay between the desired and the real velocity. This delay is between 0.3 and 0.6 seconds for all joints, providing a similar reduction in the velocity tracking performance of the manipulator joints for all three control schemes.

7. DISCUSSION

In the following section, the experimental setup and testing results will be discussed, in light of the three evaluated kinematic control schemes.

The force affecting the UVMS due to the pulley system is not identical to an underwater current, but can be seen as a virtual current force. Due to the difference between the static and dynamic friction, the force is not constant, but can be considered larger when the vehicle is stationary. Furthermore, even though the external load is actuated in the vehicle body's x-direction, the load affects the vehicle in y-direction as well, as the vehicle experiences a lot of yaw motions during the testing procedure. However, the setup still gives an impression of the kinematic control scheme and velocity tracking performance when the system is subjected
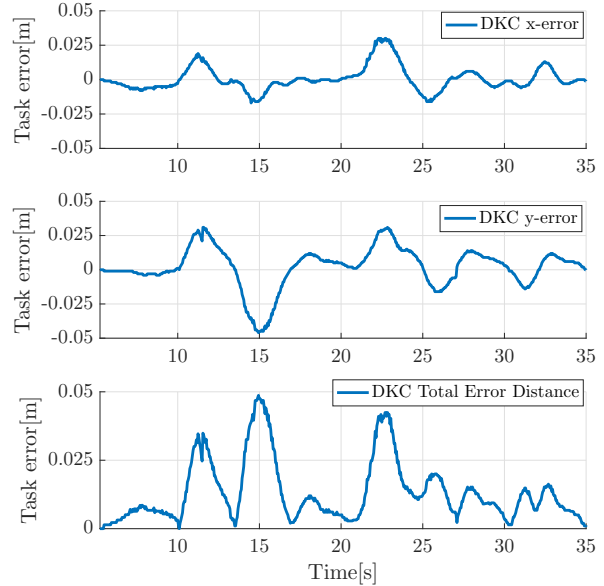
to constant underwater currents. Worth to note, the constant force of 0.53kg (approximately 5 [N]) is a realistic current force acting on the vehicle, but suddenly applying this force simulates an unrealistically large disturbance on the system. This is due to the fact that changes in the current velocity occur slowly.

Another factor limiting the effectiveness of the velocity tracking performance is related to deadband on the thrusters, and efforts could have been made to take the thruster deadband into account. For example, integral action could have been added by choosing $\boldsymbol{\Lambda} > \mathbf{0}$, although this could result in destabilizing the system. The constant additive term in the sliding mode controller counteracts the deadband, and better tuning of this term might have been possible.

The slight delay in velocity tracking for the manipulator arm is most likely due to friction in each manipulator joint. The manipulator is designed to be waterproof, thus putting demands on design of the rotating parts, especially the gaskets. Consequently, changing gasket dimensions or testing different types of lubrication may decrease friction in the manipulator arm joints.

By comparing the results for the different kinematic control schemes, it is observed that the FMKC method did not perform as well as in simulations [11]. The most plausible explanation is the delay in manipulator joint velocity tracking. The performance of FMKC compared to that of the DKC would most likely be more prominent for larger vehicle velocities. Nonetheless, when the vehicle's position and heading has stabilized, the end-effector position RMSE is below a centimeter for all the tested kinematic control schemes. This accuracy may be difficult to attain in the
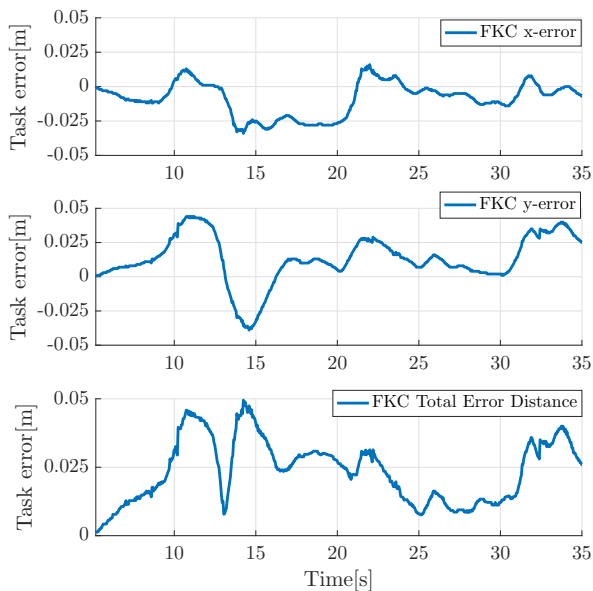
Fig. 13: A sample run showing end-effector error in x and y direction and the total error distance w.r.t. time for the FKC method.
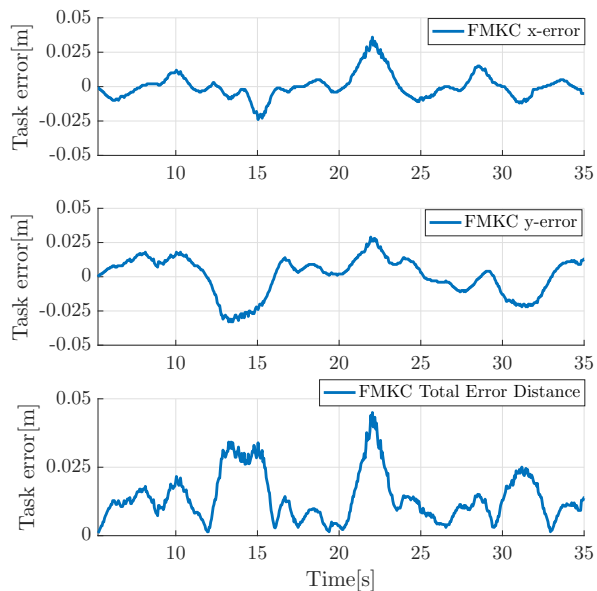
Fig. 14: A sample run showing end-effector error in x and y direction and the total error distance w.r.t. time for the FMKC method.

stabilization phase without reducing the velocity tracking delay.

Questions may be asked regarding the validity of the assumption that velocity references are followed perfectly. However, the references are followed without much delay and with little error by the manipulator arm, as can be seen in Fig. 10, and the assumption should therefore hold. For a system where there are larger delays in reference velocity tracking, such as is the case for the vehicle body in Fig. 11, this assumption is not valid. In such a system, the stability analysis should prove that the interconnected system, i.e. the interconnection between the guidance system generating velocity references and the control system, is stable. This could for instance be done with cascaded systems theory [43].

Highly accurate position and attitude measurements were provided by the QTM system at 50 Hz. However, position measurements at this update frequency and with similar precision would be difficult to come by in the ocean in a real case scenario. In such a case, estimates of position and attitude would most likely be provided by aided inertial navigation, incorporating a combination of inertial, Doppler velocity log, depth, acoustic and camera measurements. Consequently, future experiments should be performed using aided inertial navigation to estimate the states, in order to describe the performance of the system in a real scenario.

8. CONCLUSIONS

This paper considers kinematic control for underwater vehicle-manipulator systems (UVMS). Experimental validation of three kinematic control schemes has been provided. Experiments were performed using the SeaArm manipulator mounted under the BlueROV2. Two of the schemes are common solutions to the problem, and are compared to the proposed scheme for benchmarking purposes, illustrating weaknesses with the kinematic control framework. A pulley system was built and used to add a constant disturbance force on the UVMS, simulating an ocean current. Local position and attitude measurements of the UVMS body in the laboratory basin were provided by the QTM system with a Kalman filter for velocity and angular rate estimates.

The proposed and formalized control scheme named full modified kinematic control (FMKC) stabilized the end-effector, and reduced tracking error compared to the UVMS body movement significantly. It had a slightly lower RMSE for end-effector stabilization than the decoupled kinematic control (DKC) scheme, and readily outperformed the RMSE of the full kinematic control (FKC) scheme. It is argued that the delay in the velocity tracking for the manipulator arm joints was due to friction in the manipulator arm joints. The delay prevented achieving lower RMSE values in the experimental testing, and is the main reason why the RMSE difference between the schemes was smaller in simulations compared to the experimental testing. However, the need for stabilization was higher in trials with the FMKC scheme, but it still achieved the best tracking capabilities for the end-effector. It follows from the experimental testing results that all three control schemes show a high potential in keeping a desired end-effector position in an environment with disturbances such as ocean currents, and verifies that kinematic control is a promising technique for controlling an underwater vehicle-manipulator system, which is also the conclusions of [9] and especially [10].
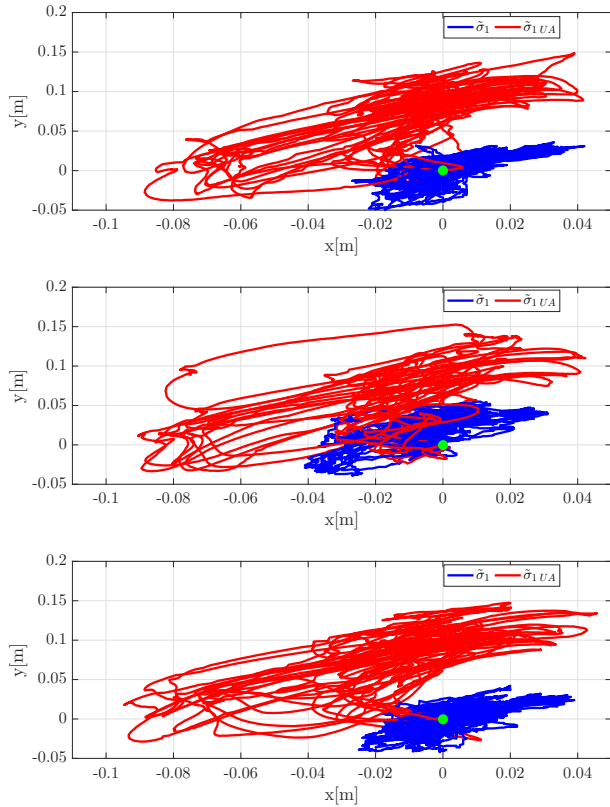
Fig. 15: End-effector position error for ten runs of the actuated ($\tilde{\sigma}_1$) and un-actuated ($\tilde{\sigma}_{UA}$) manipulator arm. The top, middle and bottom subplot show the response for the DKC, FKC and FMKC method, respectively. The point marked in green in (x,y) = (0,0) marks the zero error state.

9. ACKNOWLEDGEMENTS

REFERENCES

[1] Ingrid Schjølberg, Tor B. Gjersvik, Aksel A. Transeth, and Ingrid B. Utne. Next Generation Subsea Inspection, Maintenance and Repair Operations. *IFAC-PapersOnLine*, 49(23):434–439, 2016.

[2] Arnau Carrera, Narcís Palomeras, Natalia Hurtós, Petar Kormushev, and Marc Carreras. Learning multiple strategies to perform a valve turning with underwater currents using an i-auv. In *OCEANS 2015-Genova*, pages 1–8. IEEE, 2015.

[3] Seyed R. Ahmadzadeh, Petar Kormushev, and Darwin G. Caldwell. Autonomous robotic valve turning: A hierarchical learning approach. In *Robotics and Automation (ICRA), 2013 IEEE International Conference on*, pages 4629–4634. IEEE, 2013.

[4] Pedro J. Sanz, Pere Ridao, Gabriel Oliver, Giuseppe Casalino, Yvan Petillot, Carlos Silvestre, Claudio Melchiorri, and Alessio Turetta. Trident an european project targeted to increase the autonomy levels for underwater intervention missions. In *Oceans-San Diego, 2013*, pages 1–10. IEEE, 2013.

[5] Gianluca Antonelli. *Underwater Robots*. Springer, 2014.

[6] Stefano Chiaverini. Singularity-robust task-priority redundancy resolution for real-time kinematic control of robot manipulators. *IEEE Transactions on Robotics and Automation*, 13(3):398–410, 1997.

[7] Mark W. Spong, Seth Hutchinson, and Mathukumalli Vidyasagar. *Robot modeling and control*, volume 3. Wiley New York, 2006.

[8] Giacomo Marani, Song K. Choi, and Junku Yuh. Underwater autonomous manipulation for intervention missions AUVs. *Ocean Engineering*, 36(1):15–23, 2009.

[9] E. Simetti, F. Wanderlingh, S. Torelli, M. Bibuli, A. Odetti, G. Bruzzone, D. L. Rizzini, J. Aleotti, G. Palli, L. Moriello, and U. Scarcia. Autonomous Underwater Intervention: Experimental Results of the MARIS Project. *IEEE Journal of Oceanic Engineering*, 43(3):620–639, July 2018.

[10] Enrico Simetti, Giuseppe Casalino, Sandro Torelli, Alessandro Sperindé, and Alessio Turetta. Floating Underwater Manipulation: Developed Control Methodology and Experimental Validation within the TRIDENT Project. *J. Field Robot.*, 31(3):364–385, 2014.

[11] Erlend K. Jørgensen and Ingrid Schjølberg. Rov end-effector stabilization for unknown, time-varying currents. In *Control Conference (ECC), 2016 European*, pages 1303–1308. IEEE, 2016.

[12] Gianluca Antonelli and Stefano Chiaverini. Task-priority redundancy resolution for underwater vehicle-manipulator systems. In *Robotics and Automation, 1998. Proceedings. 1998 IEEE International Conference on*, volume 1, pages 768–773. IEEE, 1998.

[13] Nilanjan Sarkar and Tarun K. Podder. Coordinated motion planning and control of autonomous underwater vehicle-manipulator systems subject to drag optimization. *IEEE Journal of Oceanic Engineering*, 26(2):228–239, 2001.

[14] Mohan Santhakumar and Kim Jinwhan. Indirect adaptive control of an autonomous underwater vehicle-manipulator system for underwater manipulation tasks. *Ocean Engineering*, 54:233–243, 2012.

[15] Jonghui Han, Jonghoon Park, and Wan K. Chung. Robust coordinated motion control of an underwater vehicle-manipulator system with minimizing restoring moments. *Ocean Engineering*, 38(10):1197–1206, 2011.

[16] Elisabetta Cataldi and Gianluca Antonelli. Basic interaction operations for an underwater vehicle-manipulator system. In *2015 International Conference on Advanced Robotics (ICAR)*, pages 524–529.

[17] Jan-II Kang, Hyeung-Sik Choi, Bong-Huan Jun, Ngoc-Duc Nguyen, and Joon-Young Kim. Control and implementation of underwater vehicle manipulator system using zero moment point. In *2017 IEEE Underwater Technology (UT)*, pages 1–5.

[18] Dina Youakim and Pere Ridao. Motion planning survey for autonomous mobile manipulators underwater manipulator case study. *Robotics and Autonomous Systems*, 107:20–44, 2018.

[19] H. Mahesh, Junku Yuh, and R. Lakshmi. A coordinated control of an underwater vehicle and robotic manipulator. *Journal of Field Robotics*, 8(3):339–370, 1991.

[20] Thor I. Fossen and Svein I. Sagatun. Adaptive control of nonlinear systems: A case study of underwater robotic systems. *Journal of Field Robotics*, 8(3):393–412, 1991.

[21] Ingrid Schjølberg and Thor I. Fossen. Modelling and control of underwater vehicle-manipulator systems. In *in Proc. rd Conf. on Marine Craft maneuvering and control*. Citeseer, 1994.

[22] Timothy W. McLain, Stephen M. Rock, and Michael J. Lee. Experiments in the coordinated control of an underwater arm/vehicle system. *Autonomous robots*, 3(2-3):213–232, 1996.

[23] Jee-Hwan Ryu, Dong-Soo Kwon, and Pan-Mook Lee. Control of underwater manipulators mounted on an rov using base force information. In *Robotics and Automation, 2001. Proceedings 2001 ICRA. IEEE International Conference on*, volume 4, pages 3238–3243. IEEE, 2001.

[24] Donghee Kim, Hyeung-Sik Choi, Joon-Young Kim, Jong-Hyeon Park, and Ngoc-Huy Tran. Trajectory generation and sliding-mode controller design of an underwater vehicle-manipulator system with redundancy. *International Journal of Precision Engineering and Manufacturing*, 16(7):1561–1570, 2015.

[25] Mohan Santhakumar and Kim Jinwhan. Coordinated motion control in task space of an autonomous underwater vehicle–manipulator system. *Ocean Engineering*, 104:155–167, 2015.

[26] Signe Moe, Gianluca Antonelli, Andrew R. Teel, Kristin Y. Pettersen, and Johannes Schrimpf. Set-based tasks within the singularity-robust multiple task-priority inverse kinematics framework: General formulation, stability analysis, and experimental results. *Frontiers in Robotics and AI*, 3:16, 2016.

[27] Hai Huang, Qirong Tang, Hongwei Li, Le Liang, Weipo Li, and Yongjie Pang. Vehicle-manipulator system dynamic modeling and control for underwater autonomous manipulation. *Multibody System Dynamics*, 41(2):125–147, 2017.

[28] Pandurang S. Londhe, Mohan Santhakumar, Balasaheb M. Patre, and Laxman M. Waghmare. Task space control of an autonomous underwater vehicle manipulator system by robust single-input fuzzy logic control scheme. *IEEE Journal of Oceanic Engineering*, 42(1):13–28, 2017.

[29] Tae W. Kim, Giacomo Marani, and Junku Yuh. Underwater vehicle manipulators. In *Springer Handbook of Ocean Engineering*, pages 407–422. Springer, 2016.

[30] Jean-Jacques E. Slotine, Weiping Li, et al. *Applied nonlinear control*, volume 199. Prentice-Hall Englewood Cliffs, NJ, 1991.

[31] Vadim I. Utkin. *Sliding modes in control and optimization*. Springer Science & Business Media, 2013.

[32] Marc Hildebrandt, Leif Christensen, Jochen Kerdels, Jan Albiez, and Frank Kirchner. Realtime motion compensation for ROV-based teleoperated underwater manipulators. In *OCEANS '09 IEEE Bremen: Balancing Technology with Future Needs*, 2009.

[33] Hyungwon Shim, Bong H. Jun, Pan M. Lee, and Banghyun Kim. Dynamic workspace control method for underwater manipulator of floating ROV. *International Journal of Precision Engineering and Manufacturing*, 14(3):387–396, 2013.

[34] Bluerov2 webpage. https://www.bluerobotics.com/store/rov/bluerov2/. Accessed Nov. 10th, 2017.

[35] Ole A. N. Eidsvik, Bent O. Arnesen, and Ingrid Schjølberg. SeaArm - A Subsea Multi-Degree of Freedom Manipulator for Small Observation Class Remotely Operated Vehicles. *Submitted, European Control Conference (ECC), 2018 IFAC*.

[36] Thor I. Fossen. *Handbook of marine craft hydrodynamics and motion control*. John Wiley & Sons, 2011.

[37] Pål J. From, Jan T. Gravdahl, and Kristin Y. Pettersen. *Vehicle-Manipulator Systems*. Springer, 2014.

[38] Signe Moe, Andrew R. Teel, Gianluca Antonelli, and Kristin Y. Pettersen. Stability analysis for set-based control within the singularity-robust multiple task-priority inverse kinematics framework. In *2015 54th IEEE Conference on Decision and Control (CDC)*, pages 171–178.

[39] Gianluca Antonelli. Stability analysis for prioritized closed-loop inverse kinematic algorithms for redundant robotic systems. *IEEE Transactions on Robotics*, 25(5):985–994, 2009.

[40] Antonio Loría and Elena Panteley. 2 cascaded nonlinear time-varying systems: Analysis and design. In *Advanced Topics in Control Systems Theory*, pages 23–64. Springer, 2005.

[41] Marine cybernetics laboratory. https://www.ntnu.edu/imt/lab/cybernetics. Accessed Nov. 10th, 2017.

[42] Michael R. Benjamin, Henrik Schmidt, and Paul Newman. MOOS homepage. Accessed Sep. 9th, 2017.

[43] Antonio Loría and Elena Panteley. *Cascaded nonlinear time-varying systems: Analysis and design*, pages 23–64. Springer, 2005.

Bent Oddvar Arnesen Haugaløkken received his M.Sc. degree in marine technology in 2016 at the Norwegian University of Science and Technology (NTNU) in Trondheim, Norway, where he is currently pursuing his Ph.D. degree. His research areas are within development of autonomous technology for inspection, maintenance and repair (IMR) operations within the Norwegian aquaculture, with emphasis on the utilization of small-sized underwater vehicles, manipulator arms and sensor technologies.

Erlend Kvinge Jørgensen was born in 1989. He received his M.Sc. degree in control engineering in 2014, and is currently finishing his Ph.D. degree, both at the Norwegian University of Science and Technology (NTNU), Trondheim, Norway. His field of research involves increasing autonomy in underwater vehicles, more specifically navigation and control of underwater vehicles. He is currently working as an engineer within R&D in Equanostic, located in Oslo, Norway.

Ingrid Schjølberg is professor in marine technology at the Norwegian University of Science and Technology (NTNU). She is heading NTNU Oceans and is Vice Dean for Research and Innovation at Faculty of Engineering. The focus of Prof. Schjølberg's research is underwater technology mainly related to underwater inspection, maintenance and repair of underwater installations. She has worked with robotics and automation for more than 20 years and in close collaboration with the industry, such as oil and gas, manufacturing, aquaculture and process industry.